Properties of Nano-composites Based on Different Clays and Polyamide 6/Acrylonitrile Butadiene Styrene Blends

Marya Raji, Elmokhtar Essassi, Hamid Essabir, Denis Rodrigue, Abou el kacem Qaiss and Rachid Bouhfid

Abstract In the last years, serval researches have been focused on organophilic clay as reinforcements for polymer matrices. In this respect, the aim of this chapter is to valorize mineral resources; montmorillonite clay was modified using hexadecyltrimethylammonium bromide (CTAB) and then used as reinforcement in a thermoplastic copolymer matrix to compare with pristine montmorillonite and commercially organo-modified montmorillonite (Cloisite 20A). The nano-composites were prepared by melt compounding using a blend of polyamide 6 (PA6) with acrylonitrile butadiene styrene (ABS) as the matrix. Scanning electron microscopy (SEM), Fourier transform infrared spectroscopy (FTIR), thermogravimetric analysis (TGA), X-ray diffraction (XRD) as well as mechanical and rheological tests were carried out to understand the properties of these nano-composites at different particle contents. The results obtained clearly showed that the Moroccan montmorillonite was successfully modified and its addition in the selected matrix substantially improved the properties of the resulting nano-composites.

Keywords Montmorillonite · Polyamide 6 · Acrylonitrile butadiene styrene Surface modification · Nano-composites

M. Raji · H. Essabir · A. Qaiss · R. Bouhfid (✉)
Moroccan Foundation for Advanced Science, Innovation and Research (MAScIR), Laboratory of Polymer Processing, Institute of Nanomaterials and Nanotechnology (NANOTECH), Rabat, Morocco
e-mail: r.bouhfid@mascir.com

M. Raji · E. Essassi
Laboratory of Organic Chemistry and Heterocyclic, Faculty of Science, Mohammed V University, Rabat, Morocco

D. Rodrigue
Department of Chemical Engineering and CERMA, Université Laval, Quebec City G1V0A6, Canada

M. L. Sanyang and M. Jawaid (eds.), *Bio-based Polymers and Nanocomposites*,
https://doi.org/10.1007/978-3-030-05825-8_6

1 Introduction

In recent years, polymer nano-composite has been a topic of high scientific research and industrial development (Zeng et al. 2005), especially for several applications like automotive (Raji et al. 2016b), aerospace (Raji et al. 2017b), construction (Essabir et al. 2016b), and packing (Zari et al. 2018). This interest is related to their excellent specific properties such as mechanical properties (Raji et al. 2016a) and thermal stability (Raji et al. 2017a). This kind of materials can be produced using either by thermoplastics (Laaziz et al. 2017), thermosets, or elastomers (Abdellaoui et al. 2017) filled by low content of nano-sized particles (less than 100 nm) (Gacitua et al. 2005). The incorporation of these small particles into a polymer matrix can also decrease the cost of materials (Wang et al. 2013) and its impact on the environment (Essabir et al. 2016a). The nanoparticles can be synthetic or natural (Bensalah et al. 2017; Boujmal et al. 2017). Typical examples of natural nanoparticles are layered materials such as graphene (Pretschuh et al. 2014), silicate (Vuluga et al. 2014), and clays (Bhattacharya and Aadhar 2014)), or fiber-like materials such as carbon nano-tubes and nano-fibers (Nuzzo et al. 2014), sepiolite (Mejía et al. 2014; Zotti et al. 2014), or cellulose nano-fibers (Erden and Ho 2017).

Inorganic resources as nanoparticle fillers are being exploited substantially as an alternative to organic and synthetic materials because of their high in-plane strength and stiffness, rich intercalation chemistry as well as their abundance in nature and availability. Among them, the use of clay nanoparticles is attracting ever-growing interest due to its large aspect ratio and their unique layered structure (Leszczy et al. 2007) and high surface area (Amendola et al. 2012). The excellent properties of polymer nano-composite reinforced with clays (Singla et al. 2012) led to substantial mechanical (Usuki 2002) and thermal stability (Gao 2004) improvement. They also decrease gas and liquid permeability (Bergaya and Lagaly 2013). Moreover, they were shown to improve flame retardancy (Laoutid et al. 2013), without affecting the optical properties of the base polymer (Navrátilová et al. 2007). But their main advantage is to improve the rigidity of a neat polymer (Wang et al. 2013).

2 Clay Minerals: Structure, Modifications, and Properties

2.1 Clay Structure

The word “clay” has ambivalent definitions. On the first hand, in terms of simple definitions relating to geological knowledge, it is used to define any fine-grained fraction of rocks, sediments, and soil particles less than 2 μm in equivalent spherical diameter. On the other hand and from the chemical knowledge, this word includes a large group of hydrated phyllosilicates. Roughly speaking, clay minerals are essentially microcrystalline secondary minerals based on hydrous magnesium or aluminum silicates and carry negative charges that have sheet-like structures with

Table 1 Classification of planar 2:1 phyllosilicates (Guggenheim et al. 2006)

Layer charge[a]	Interlayer material	Group	Octahedral character	Example of species
0	None	Talc-Pyrophyllite	Trioctahedral Dioctahedral	Talc-pyrophyllite
0.4–1.2	Hydrated exchangeable cations	Smectite	Trioctahedral Dioctahedral	Saponite Montmorillonite
1.2–1.8	Hydrated exchangeable cations	Vermiculite	Trioctahedral Dioctahedral	Vermiculite Vermiculite
1.7–2.0	Non-hydrated monovalent (>50%) cations	True(Flexible) Mica	Trioctahedral Dioctahedral	Phlogopite Muscovite
1.2–1.7	Non-hydrated mono- or divalent cations	Interlayer-deficient Mica	Trioctahedral Dioctahedral	Illite Wonesite
2.6–4.0	Non-hydrated or divalent (>50%) cations	Brittle Mica	Trioctahedral Dioctahedral	Clintonite Margarite
variable	Hydroxide sheet	Chlorite	Trioctahedral Dioctahedral Di, Trioctahedral	Clinochlore Donbassite Cookeite

[a]Approximate negative net charge per anionic $O_{22}(OH)_4$ formula unit

very fine particle size and a general chemical formula (Ca, Na, H)(Al, Mg, Fe, Zn)$_2$(Si, Al)$_4$O$_{10}$(OH)$_2$–xH$_2$O, where x represents the variable amount of water.

Generally, the different structures of clay minerals are basically composed of two basic units: the silica tetrahedron "SiO_2" and alumina octahedron "AlO_6" at different ratios; (*i*) In 1:1 ratio, this structure is based on one octahedral sheet linked to one tetrahedral sheet as Kaolinite (González and Del 2006), Halloysite (Zhao et al. 2013), etc. (*ii*) In 2:1 ratio, this structure is created from two tetrahedral sheets sandwiching an octahedral sheet that is classified into separate groups on the basis of the layer charge and interlayer material (Tian and Tagaya 2007); see Table 1.

Montmorillonite (MMT) as one of the most popular inorganic fillers, a member of the smectite family, is classified into the general family of 2:1-layered silicates (Carrado 2000), identified with the chemical formula $M_x(Al_2{-}xMg_x)Si_4O_{10}(OH)_2 \cdot nH_2O$ (Laoutid et al. 2013). Its crystal structure is composed of nanometer-thick layers based on alumina octahedral sheets sandwiched between two silica tetrahedral sheets (Majeed et al. 2013). They are also characterized by the presence of cations in between layers (Na^+, K^+, Ca^+, etc.) (Tamura et al. 2008). This type of clay is characterized by its easy availability, low density, and its low cost-effectiveness (Jeong et al. 2011).

2.2 Problematic

Montmorillonite like as all types of clay is naturally hydrophilic (Oliveira and Machado 2013). This character makes them difficult to mix and interact with most polymer matrices which are hydrophobic (Nekhlaoui et al. 2014). For these reasons, montmorillonite must be surface-treated before their introduction into a polymer matrix to make high-quality nano-composites by ensuring good dispersion and interfacial adhesion (de Paiva et al. 2008).

2.3 MMT Modifications

Generally, clay surface can be modified by organic compounds based on the exchange of sodium cations located within the interlayer's or in the galleries with organic cations (Donescu et al. 2008) (Fig. 1). The most commonly used are alkyl ammonium (Tamura et al. 2008), sulfonium (Majeed et al. 2013), and phosphonium (Nazir et al. 2016) ions. This substitution changes the hydrophilic silicate surface to an organophilic one (Raji et al. 2016b). It also increases the gallery spacing (*d*-spacing) between the layers (Kumar et al. 2010; Mansoori et al. 2012). For example, Cloisite 20A is a commercially organo-modified montmorillonite intercalated with dimethyl, dehydrogenated tallow quaternary ammonium (2M2HT), where HT is the hydrogenated tallow (∼65% C18, ∼30% C16, and ∼5% C14) (Bhat et al. 2008; Diagne et al. 2006; Tjong 2006). But the modification depends on the cation-exchange capacity of the layers (de Paiva et al. 2008), as well as the content and structure of the surfactant and the way the surfactant molecules organize themselves in the clay (Fujimori et al. 2010).

The synthesis of organo-modified montmorillonite was carried out by intercalating the clay layers with a long-chain organic surfactant. The preparation was done by solubilization of hexadecyltrimethylammonium bromide ($[H_3C\ (H_2C)_{15}–N^+–(CH_3)_3]\ Br^-$) in ethanol. This surfactant solution was then slowly added to the clay suspension obtained by the dispersion of (MMT-Na) in water:ethanol (1:1) at 80 °C under continued high-intensity stirring. Finally, centrifugation was used to separate the organo-modified clay. The particles were washed five times with a water:ethanol (1:1) solution to remove any residues. The general reaction for MMT modification is shown in Eq. 1:

$$Na^+ - Clay + HOOC - R - NH_3 + Cl^- \rightarrow HOOC - R - NH_3^+ - Clay + NaCl \quad (1)$$

2.4 MMT Properties

2.4.1 Structural Properties

- ***X-ray diffraction (DRX)***

Wide-angle X-ray diffraction (WAXD) was used to identify the chemical composition and crystallographic structure of the clays. The measurements were carried out on a Bruker D8 Discover using the Cu Kα radiation (λ = 0.154184 nm) and a GADDS detector. The samples were consolidated in an aluminum holder and scanned at 45 kW from 2° to 10° of 2θ. The diffraction patterns were analyzed using the X'Pert High Score software (Fig. 2).

Figure 2 shows the XRD pattern of MMT-Na and organo-modified clay MMT-CTAB. Both clays display a broadband in the region between 2θ = 6.16° and 2θ = 4°, respectively. The interlayer spacing corresponding of the peak of MMT-Na around 1.43 nm which increased to 2.2 nm for the organo-modified clay is getting close to that of Cloisite 20A (d = 2.84 nm calculated using the large band at 3.1°), according to Bragg's equation (Kumar et al. 2010). It can be concluded that, after clay modification by the organic surfactant, intercalation between the silicates layers occurred. This intercalation constitutes an efficient way to increase surface hydrophobicity which is a fundamental prerequisite for good compatibility between the polymer matrix and the montmorillonite surface (Agag et al. 2001). It also increases the distance between each layer (d-spacing).

- ***Fourier transforms infrared spectra (FTIR)***

Fourier transform infrared spectra (FTIR) of the different clays and nano-composites were recorded using an ABB Bomem FTLA 2000-102 spectrometer (ATR: SPECAC GOLDEN GATE). The spectra were obtained by an accumulation of 16 scans and a resolution of 4 cm^{-1}.

The FTIR spectra of MMT-Na, Cloisite 20A, and MMT-CTAB are presented in Fig. 3. The bands around 3600 and 3400 cm^{-1} are indicative of montmorillonite in all spectrums, which can be attributed to O–H stretching for the silicate and water

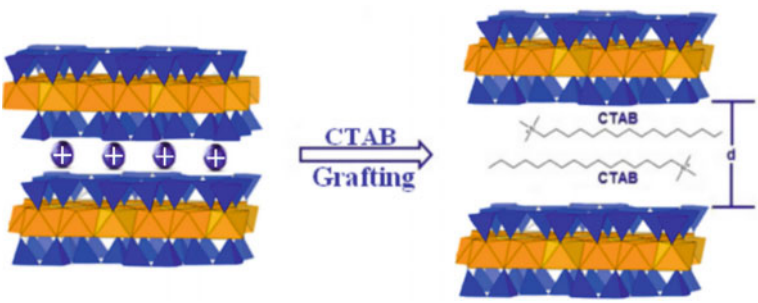

Fig. 1 Schematic of synthetic procedure for MMT-CTAB

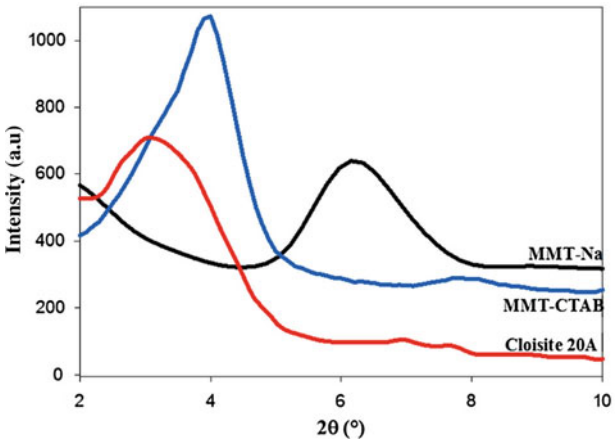

Fig. 2 XRD patterns of MMT-Na and modified MMT

(Kumar et al. 2010). In the FTIR spectrum of MMT-CTAB appears a band in the region of 1645 cm^{-1} is attributed to the –OH bending mode of the adsorbed water (Kumar et al. 2010). The characteristic band at 1134 cm^{-1} is assigned to Si–O stretching and out-of-plane Si–O stretching mode of montmorillonite (Yürüdü et al. 2005). The band at 1004 cm^{-1} is ascribed to Si–O stretching (in-plane) vibration for layered silicates (Xie et al. 2011). The IR bands at 945, 814, and 719 cm^{-1} are attributed to Al–Al–OH, Al–Fe–OH, and Al–Mg–OH bending vibrations, respectively (Navrátilová et al. 2007; Xie et al. 2011; Xue et al. 2007). Moreover, the –OH bending mode band of adsorbed water at 1645 cm^{-1} in the MMT-Na spectrum has a lower intensity because the absorbed water in MMT-CTAB is more limited due to the presence of the organic cations (Kumar et al. 2010). In addition, the bands at 1470 and at 1416 cm^{-1} are assigned to H–C–H and C–N stretching vibrations, respectively (Kumar et al. 2010). Figure 3 also presents two weaker bands as a doublet at 3054 and at 3028 cm^{-1} which can be associated to the C–H bonds of aromatic stretching vibrations normally present in CTAB (Gavrilko et al. 2013; Aowda et al. 2011). Finally, the presence of CTAB in the MMT-CTAB spectrum is confirmed, which implies that CTAB has been intercalated into the MMT-Na structure (nano-space inside montmorillonite).

In the FTIR spectrum of Cloisite 20A (Fig. 3), the transmittance bands at 1040 and 916 cm^{-1} are due to the stretching vibration of Si–O–Si from silicate and to the Al–OH–Al deformation of aluminates, respectively. Another band at 726 cm^{-1} belongs to Si–O stretching of quartz and silica. Finally, the transmittance bands between 600 and 400 cm^{-1} can be associated with the Al–O stretching and Si–O bending vibrations. In addition to the bands observed for montmorillonite, the bands located at 2930 and 2856 cm^{-1} can be assigned to the asymmetric and

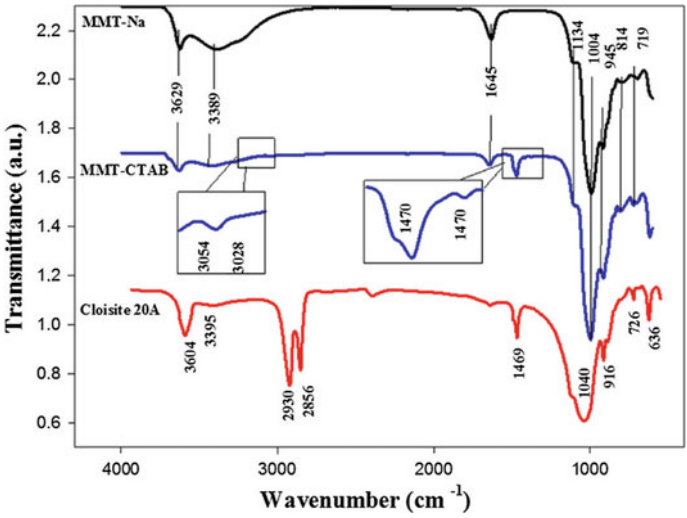

Fig. 3 FTIR spectra of MMT-Na, organo-modified clay (MMT-CTAB), and Cloisite 20A particles

symmetric vibrations of the methylene groups (CH_2) from surfactant molecules (long aliphatic chains), and the band at 1469 cm^{-1} may be ascribed to the asymmetric deformation vibrations of $–CH_3$ of the aliphatic chain of the surfactant (Navrátilová et al. 2007).

2.4.2 Morphological Properties

- ***Scanning electron microscopy*** **(*SEM*)**

Montmorillonite powder was subjected to scanning electron microscopy (SEM) to investigate the morphology of their granules. Small amount of montmorillonite powder was poured on the carbon tape, and then, the excess was blown with air gun to ensure that small pieces of the powder remain on the tape.

The shapes of the Montmorillonite were studied by scanning electron microscopy (SEM). A general view using the micrographs of the clay powder can be observed in Fig. 4. Nevertheless, the stronger nanoparticles intermolecular interactions, that is, a cohesive tension make an attempt to the clay particles to aggregate and to form the agglomerates (Akin and Tihminlioglu 2018). Figure 4 shows that the montmorillonite possesses a plate-like morphology with nanometric size.

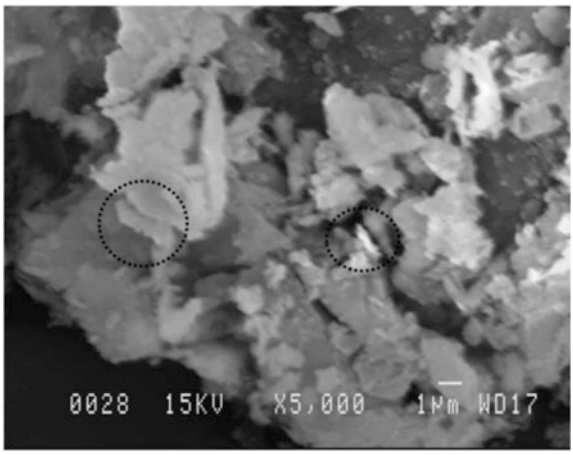

Fig. 4 SEM images of montmorillonite clay

2.4.3 Thermal Properties

- ***Thermogravimetric analysis*** **(*TGA*)**

Thermal stability plays an essential role in determining the technical applications of composite materials. For this reason, TGA was used to compare the degradation profiles of the different types of clay used (MMT-Na, MMT-CTAB, and Cloisite 20A) and the results are presented in Fig. 5.

Figure 5 shows that the thermal decomposition of MMT-Na occurs in two steps: The first one around 82 °C (14% weight loss) is due to free water and interlayer water residing between the aluminosilicate layers and related to the hydration spheres of the cations (Carastan et al. 2013), while the second weight loss between 500 and 700 °C (2% weight loss) is due to dehydroxylation of the aluminosilicate lattice (Xie et al. 2011). On the other hand, the decomposition curves of the organoclay can be divided into four parts: (1) The free water region below 200 °C

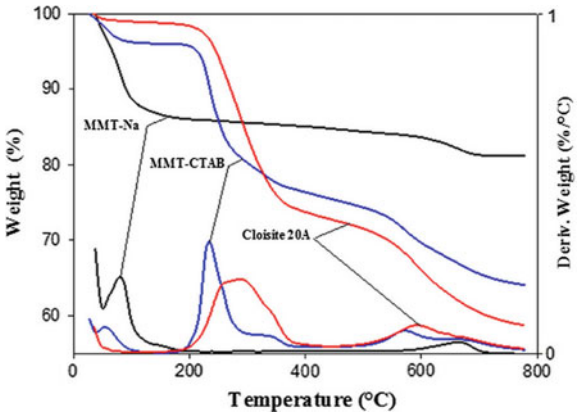

Fig. 5 TGA and DTG curves for the different clays used (Cloisite 20A, MMT-CTAB, and MMT-Na)

is characterized by a weight loss of 5% in MMT-CTAB which is lower than of MMT-Na (Pavlidou and Papaspyrides 2008). (2) The region where the CTAB and all organic substances thermally decompose is around of 231 °C with a total weight loss of 23% (Wu and Chen 2004) such region is also present for Cloisite 20A at 288 °C (26% loss) (Hoidy and Al-mulla 2013). This again confirms the intercalation of MMT-Na by CTAB as determined by XRD. (3) A weight loss of 3% due to water in the interlayer space is usually removed around 336 °C for MMT-CTAB (Wu and Chen 2004). Finally, (4) both of evaporation and complete decomposition of organic and inorganic moieties in the surfactant (Zhang et al. 2013), as well as dehydroxylation of the aluminosilicate lattice, was observed around 593 °C for Cloisite 20A (weight loss 3%) and around 600 °C for MMT-CTAB (weight loss 2%), respectively, which are lower than for MMT-Na. This behavior is associated to the presence of organic substances having a direct effect on decomposition (Zhang et al. 2013), depending on the number of the carbon chains acting as energy sources leading to further decomposition (Kokal et al. 2011). FTIR results also confirmed the presence of organic molecules in MMT-CTAB and Cloisite 20A. One can, therefore, conclude that MMT-CTAB exhibits excellent thermal stability compared to MMT-Na and close to that of Cloisite 20A, confirming again that intercalation of MMT-Na by the surfactant was successful (Pavlidou and Papaspyrides 2008).

The grafted yield (%), which corresponds to the number of intercalated molecules which effectively participated in the coupling reaction, can be determined using the weight loss between 200 and 800 °C corresponding to surfactant degradation (MMT-CTAB and Cloisite 20A). The results show that the amount is around 21 and 30%, respectively.

3 Organo-Modified Clay Nano-composite Preparation

3.1 Problematic

As for as any composite materials, the properties of nano-composites mostly depend on the dispersion distribution of the particles in the polymer matrix. For this reason, various methods were developed to compound montmorillonite such as: in situ polymerization (Hakeem et al. 2014), solution blending (He et al. 2010), and melt blending (Raji et al. 2016a). But most processes use the latter because it is cost-effective and can produce homogeneous compounds with good dispersion/distribution at large scale (Šupová et al. 2011).

3.2 Nano-composites Preparation

The objective of this chapter is to compare the morphological, thermal, rheological, and mechanical properties of polymers nano-composite based on different

nanoparticles: pristine and modified montmorillonite, as well as commercially available Cloisite 20A. The nano-composites are based on unmodified montmorillonite (MMT-Na), organo-modified montmorillonite (MMT-CTAB) by adding hexadecyltrimethylammonium bromide (CTAB) as a surfactant, and three different montmorillonite clays: unmodified clay (PA6/MMT-Na), organoclay (PA6/MMT-CTAB) composite and commercially clay (Cloisite 20A) nano-composite. In all cases, the nanoparticles were first dispersed into polyamide 6 (masterbatches) and then compounded with acrylonitrile butadiene styrene (ABS) to get the final nano-composites by means of a simple melt compounding via a Leistritz ZSE-18 twin-screw extruder (Leistritz Extrusiontechnik GmbH, Germany), under the following conditions: a constant barrel temperature of 240 °C with 220 °C for the die. In general, different amounts (1, 2, 3, 4, and 5% wt.) of each nano-clay were incorporate into ABS using three different masterbatches (10% wt. nanoparticles) obtained by the combination of PA6 with either MMT-Na, MMT-CTAB, and Cloisite 20A. After extrusion and pelletizing in a precision grinder (FRITSCH Pulverisette 19) into pieces of 2–3 mm, the compounds were injection molded using an Engel e-Victory injection molding machine with a 40 tons platen capacity. The process temperature was fixed at 240 °C in the barrel and at 220 °C at the nozzle, while the mold was maintained at 45 °C (Bensalah et al. 2017). Then, the (ABS/PA6/MMT-Na), (ABS/PA6/MMT-CTAB) and (ABS/PA6/Cloisite 20A) nano-composites were tested using different characterization methods as described next. A schematic representation of the preparation methods is given in Fig. 6.

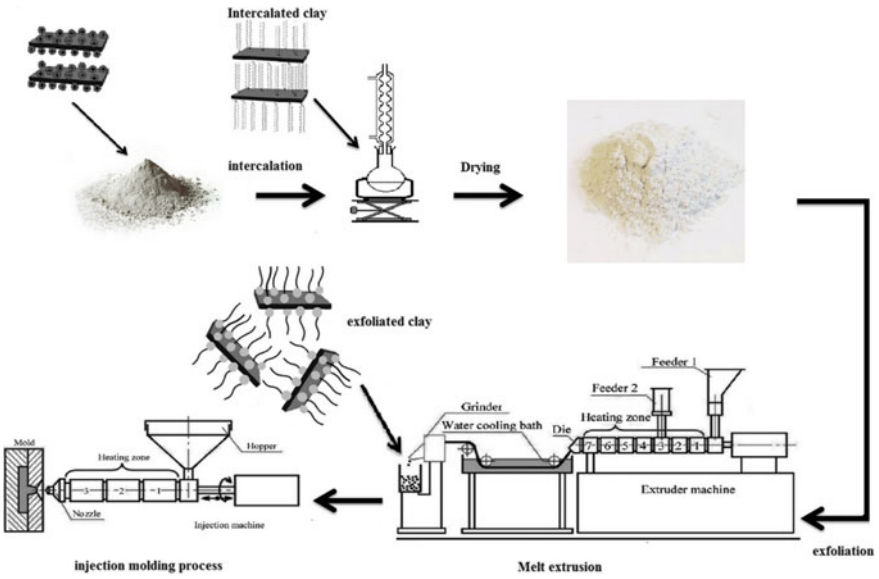

Fig. 6 Schematic representation of the preparation method for the polymer clay nano-composites produced

4 Nano-composites Properties

4.1 Morphological Properties

- ***Scanning electron microscopy* (*SEM*)**

Scanning electron microscopy (SEM) constitutes an efficient tool to investigate the morphology of the nano-sized clays dispersion/distribution in the copolymer matrix. To obtain clean and accurate fractures, all the composites were cry fractured in liquid nitrogen.

Figure 7 shows the SEM images of the cryo-fracture surface of the nano-composites of ABS-PA6/Cloisite 20A, ABS-PA6/MMT-CTAB, and of ABS-PA6/MMT-Na containing 3 wt% clay content. The micrographs of clay nano-composites presented in Fig. 7a, b, c show typical co-continuous morphologies, an ideal model for high performance multi-component polymeric materials, in which the ABS (50%) domains presented by the white regions dispersed in the PA6 (47%) matrix, illustrated by the black part, these two immiscible polymers are combined together to form one system (Essabir et al. 2017; Li and Shimizu 2005). It's clearly observed that the gray parts correspond to the organoclay particles are located in PA6 phase, this phenomenon is due to the significant effect of exfoliated clay platelets on the rheological behavior of polymers, more precisely, the preferential location of the organoclay in the PA6 phase can significantly increase its viscosity and prevent the coalescence of the dispersed phase during extrusion (Yan et al. 2012). The selective localization of the clay existing in the PA6 phase is due to the different affinities between the organoclay and the two polymers (Yan et al. 2012). The clay layers are easily exfoliated by PA6 molecular chains compared to ABS molecular chains because of the higher polarity of the PA6 chains (Li and Shimizu 2005).

It's seen also from the Fig. 4 that the clay particles in the PA6 polymer formed a small aggregates, with the average of nanometer-size particles was around of 260, 195 and 459 nm correspond to Cloisite 20A, MMT-CTAB, and MMT-Na, respectively, this variation of the aggregates size, clearly indicates that the particles in MMT-Na clay before the treatment was in closely attached or in aggregates form due to the intermolecular forces and then in the presence of cationic surfactant, the clay particles are highly exfoliated into small aggregates, this may be due to the sodium ions in the interlayer spaces of clay can be exchanged for an amino acid such as CTAB (Zýková et al. 2009). In addition, it's clear that the organoclay composites surface appear to be covered by PA6 polymer. So, the interfacial adhesion in the presence of cationic surfactant into the interlayer spaces has been improved.

It's clear on Fig. 4 that the clays particles are uniformly dispersed in the matrix with small amount of agglomerates in the case of the MMT-Na composite, attesting that the use of melt compounding process to manufacture different types of composites is evident and enabled better particles distribution.

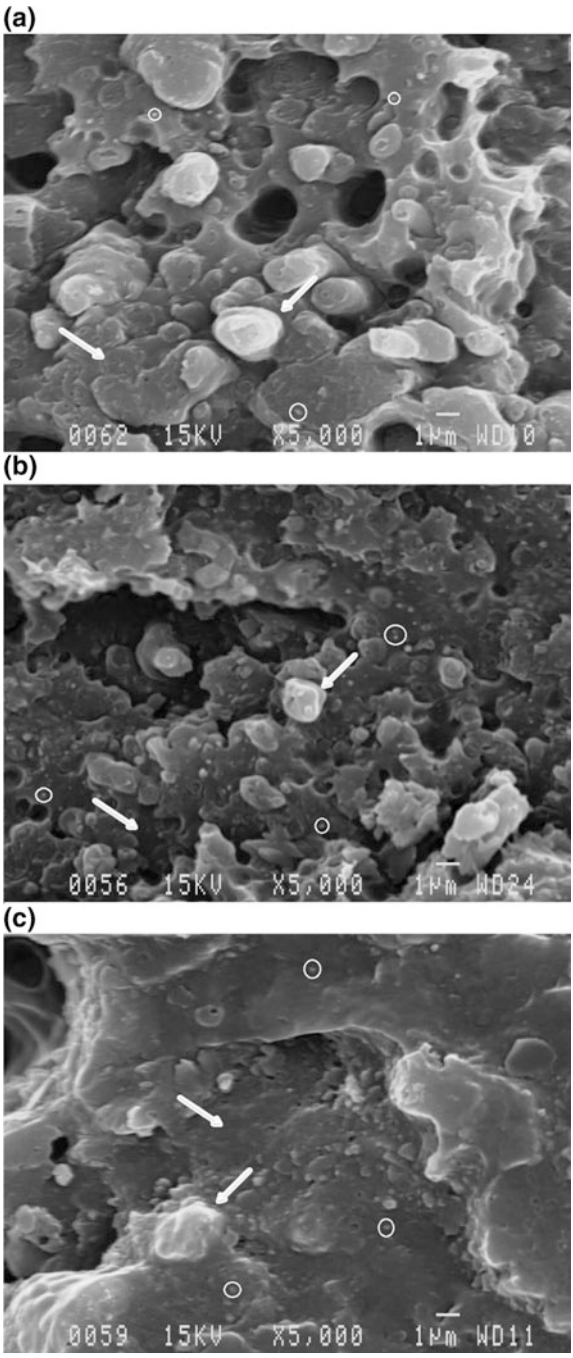

Fig. 7 SEM images of composites based on ABS-PA6 and of **a** 3 wt% of Cloisite 20A, **b** 3 wt% of MMT-CTAB, and **c** 3 wt% of MMT-Na

4.2 Thermal Properties

- ***Thermogravimetric analysis*** **(*TGA*)**

The thermal degradation of the different clays and nano-composites was evaluated by thermogravimetric analysis (TGA) using a model Q5000 from TA Instruments. Roughly 20 mg of each sample was placed in a platinum pan and heated under air from room temperature to 800 °C at a heating rate of 10 °C/min to yield the onset decomposition temperature.

Typical thermogravimetric curves of the nano-composite filled with different amounts of clay nanoparticles are presented in Fig. 8. All the curves exhibited a one-step degradation which is attributed to the random radical scission mechanism of polyolefin's degradation (Albano et al. 1999). The addition of clay increased the degradation temperature of ABS/PA6/Clay nano-composite because clay has a much higher decomposition temperature than the polymer matrix (Santos et al. 2013). Furthermore, the thermal stability of ABS/PA6/Clay nano-composite increased with clay loading.

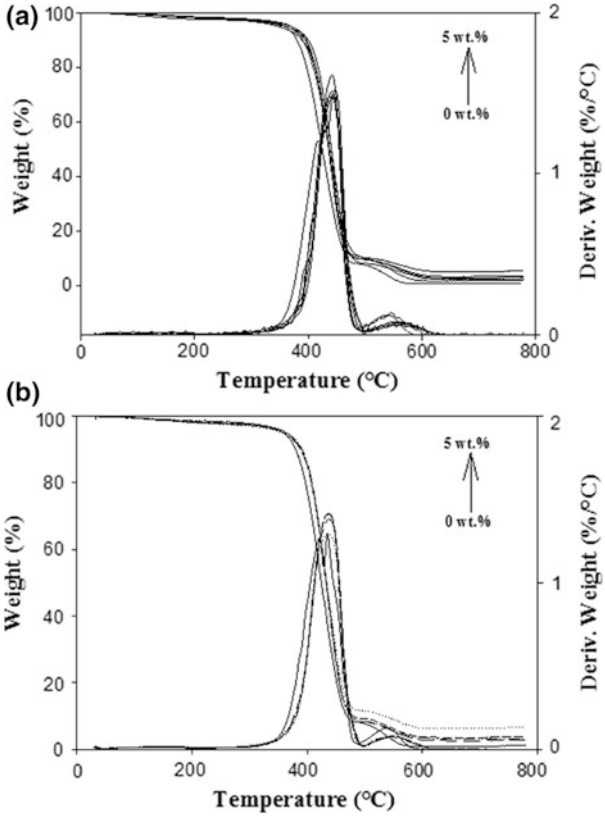

Fig. 8 TGA and DTG curves for: **a** the different nano-composites based on MMT-Na, and **b** the different nano-composite based on Cloisite 20A

Table 2 Temperature corresponding to a weight loss of 5% (T5%), 10% (T10%), 15% (T15%), and 20% (T20%) from TGA measurements of ABS/PA6/MMT nano-composite with various MMT-Na and Cloisite 20A contents

	Decomposition temperature for MMT-Na (°C)				Decomposition temperature for Cloisite 20A (°C)			
Clay content (wt%)	T5%	T10%	T15%	T20%	T5%	T10%	T15%	T20%
0	356	380	390	397	356	380	390	397
1	356	390	401	408	356	388	400	407
2	357	394	405	412	357	388	400	407
3	369	397	406	412	364	389	401	408
4	367	394	406	413	360	389	401	408
5	368	399	410	417	364	391	401	408

The temperatures corresponding to different weight loss are listed in Table 2 and it is clear that a direct relation between these temperatures and nano-clay loading exists. Furthermore, the highest thermal stability was observed for the MMT-Na and Cloisite 20A at 5% wt. and their T5, T10, T15, and T20% are about 12, 19, 20, 20 °C and 8, 11, 11, 11 °C higher than for the neat matrix, respectively. This can be explained by the effect of clays acting as thermal insulators and mass transport barriers to improving thermal stability (Bidsorkhi et al. 2014; Tartaglione et al. 2008). Thermal stability improvement is a direct effect of the excellent thermal barrier effect provided by the layered clays within the matrix. So, the better thermal stability of the nano-composites can be attributed to the clay layered structure limiting the mobility of small molecules produced during thermal decomposition. Furthermore, the thermal stability of MMT-Na is higher than Cloisite 20A due to a large number of grafted carbon chains present in the surfactant. These carbon chains acted as energy sources helping the samples to further decompose (Kokal et al. 2011).

4.3 Mechanical Properties

Dynamic mechanic analysis (DMA) and dynamic mechanical thermal analysis (DMTA) were performed using a Rheometer Solid Analyzer (RSA) according to ASTM D4092-01 (ASTM D 4092 – 01 2013). Due to the stiffness of the studied materials, a dual cantilever configuration was used. In DMA, a sinusoidal mechanical excitation is applied from which the force, deformation, and phase angle shift between the force and deformation were obtained as a function of frequency. The frequency sweeps ranged from 0.015 to 15 Hz with a strain of 0.002 (linear region of the materials). Similar conditions were used for dynamic mechanical thermal tests (DMTA) by heating the samples from 20 to 200 °C at a heating rate of 10 °C/min.

- ***Dynamic mechanical analysis (DMA)***

The complex modulus of the MMT-Na, MMT-CTAB, and Cloisite 20A nano-composites has been plotted as a function of nanoparticle content in Fig. 9. It can be seen that the complex modulus of MMT-Na, MMT-CTAB, and Cloisite 20A increased significantly with clay addition. This behavior can be associated to reinforcing effects through the formation of efficient and strong interactions between the polymer chains and the clay galleries at the interface which enhanced the compatibility between the phases (modified filler) (Hakeem et al. 2014). This can also be attributed to the incorporation of rigid particles changing the local molecular dynamics (lower polymer chain mobility) (Laaziz et al. 2017). Moreover, the frequency has also an effect on the composites response since the materials are viscoelastic. It is clear from Fig. 9 that E^* increases with increasing frequencies for the range of conditions tested (0.015–15 Hz).

- ***Dynamic mechanical thermal analysis (DMTA)***

The glass transition temperature of the composite, as obtained from the maximum of the damping factor ($\tan\delta = G''/G'$) curves using dynamic mechanical thermal analysis, is presented in Fig. 10. A clear decrease from 0 up to 4% wt. is observed: about 1.6 °C for Cloisite 20A and MMT-CTAB. Then, a slight increase is observed at 5% wt. suggesting that the mobility of the bulk polymer chains is restricted by the presence of the nanoparticles and related to their content (Santos et al. 2013). For MMT-Na, the glass transition temperature Tg decreases continuously by about 1.0 °C from 0 to 5% wt. The addition of low nano-clay content slightly decreased the glass transition temperature of the composite because the silicate layers can act as nucleating agents in the polymer matrix (Pavlidou and Papaspyrides 2008), which can also improve spherulites growth (Fragiadakis et al. 2005). At 4% wt., a high number of crystallites are formed, and the addition of more clay did not change the crystal structure of the polymer since no more space for the polymer molecules to reorganize is available inside the matrix. But nucleation and growth efficiency depend on clay dispersion.

4.4 Rheological Properties

- ***Melt rheological test***

Melt rheology tests were performed on an MCR 500 (Physica) Rheometer equipped with a CTD600 device. The measurements were carried out at 240 °C under small amplitude oscillatory shear mode using 25 mm parallel plate–plate geometry with 2-mm-thick samples. Frequency sweeps between 500 and 0.05 Hz were performed at a strain of 5%, for which the materials exhibit a linear viscoelastic behavior as verified by previous strain sweeps.

The rheological properties of the nano-composites were also investigated in the melt state, and the results are plotted in Fig. 11. It can be seen in Fig. 11a that the

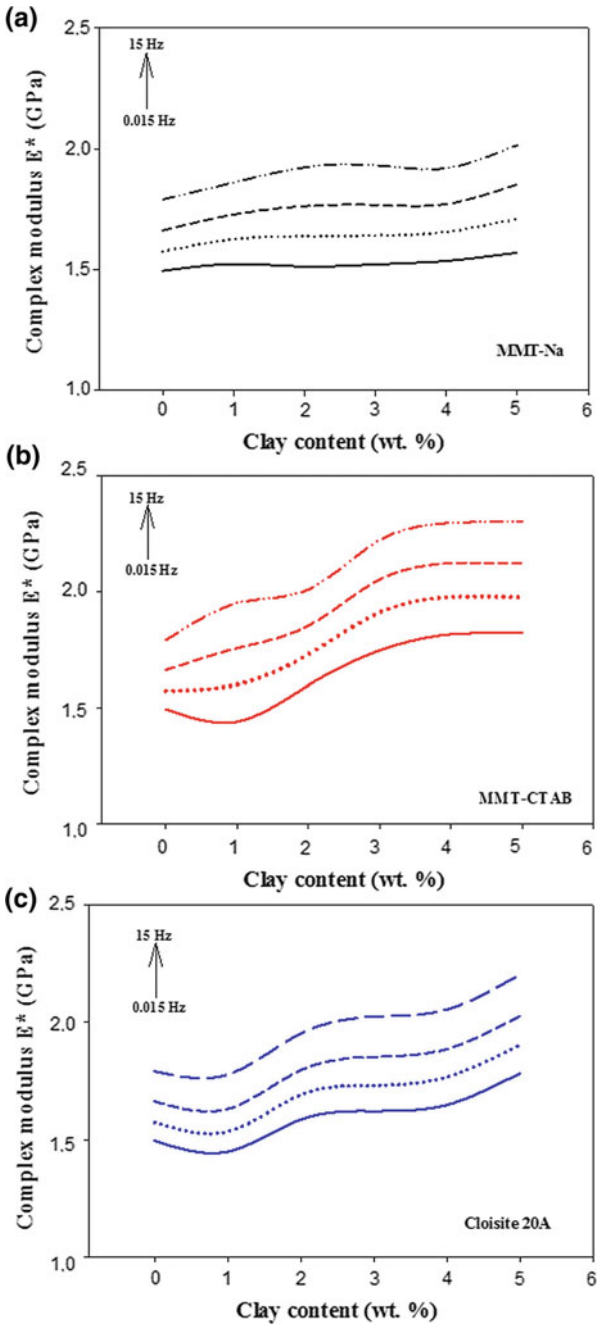

Fig. 9 Complex modulus as a function of nanoparticle content for different frequency: **a** MMT-Na, **b** MMT-CTAB, and **c** Cloisite 20A

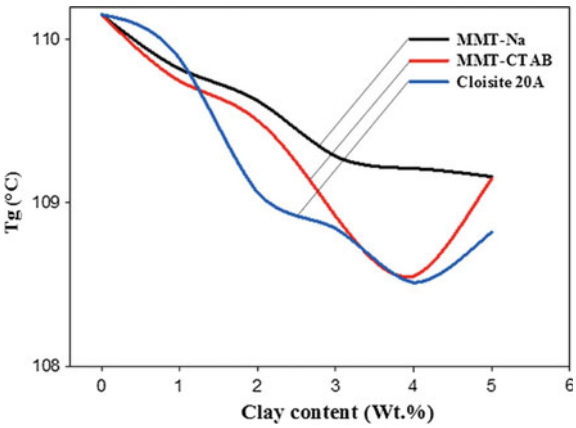

Fig. 10 Glass transition temperature (T_g) for the different nano-composites as a function of clay content

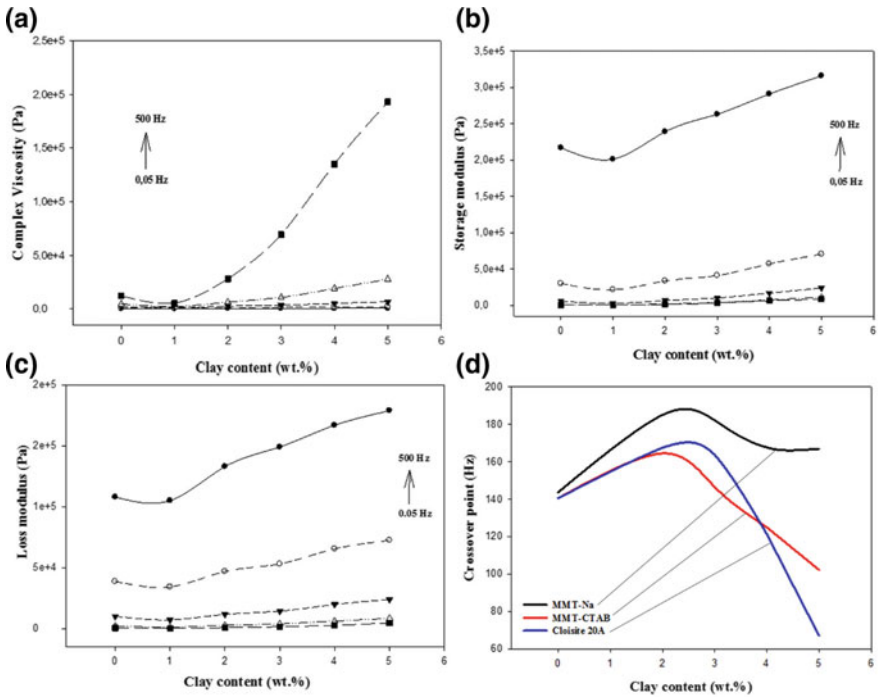

Fig. 11 Dynamic rheological properties of the nano-composites (240 °C) as a function of clay content: **a** complex viscosity, **b** storage modulus (G′), **c** loss modulus (G″), and **d** crossover point

complex viscosities of the clay composites have a plateau at low frequency or the Newtonian behavior, indicating a transition from a liquid-like to a solid-like viscoelastic behavior. Then, Fig. 11b shows that the nano-clay particles increase the storage moduli, indicating that the rheological properties of the reinforced copolymer were mainly influenced by the addition of nano-clay, and at higher clay content, the elastic character of the material prevails over its viscous behavior (Bensalah et al. 2017).

Figure 11c shows the loss modulus against frequency for various nano-clay contents. An increase in loss modulus with increasing MMT-CTAB content can clearly be observed when the nano-clay content increases over the whole frequency range. Due to good dispersion, distribution, and affinity of the rigid nano-clay inside the polymer blend, all these phenomena can prevent the melt to flow which is reflected by an increase in loss modulus/viscosity (Yürüdü et al. 2005).

Finally, Fig. 11d shows the variation of the crossover point (frequency where $G' = G''$) with clay content. The results show a decrease in the crossover point values until a maximum presented at 5 wt% of MMT-CTAB content. This reduction in crossover frequency indicates that G'' becomes smaller than G' or the materials have lower elasticity and lower energy dissipation. This behavior can be associated with insufficient time to allow for polymer chains to relax with increasing rigid particle content, which is a contribution from the increased elastic nature of the polymer melt (Raji et al. 2016b).

5 Conclusion

In summary, the montmorillonite can be successfully modified using hexadecyltrimethylammonium bromide (CTAB). The XRD and FTIR results clearly showed that intercalation of the organic cationic surfactant between the clay mineral layers occurred. The modified clay was then used as reinforcement inside a thermoplastic copolymer matrix based on polyamide 6/acrylonitrile butadiene styrene. The results were compared with the unmodified clay (MMT-Na) and a commercial organoclay (Cloisite 20A). The compounds were prepared by twin-screw extrusion, and the samples were molded via injection molding. For the nano-composites produced under the range of conditions tested (0–5% wt.), it was found that exfoliated clay platelets were selectively localized in the PA6 phase and also was found that 4% wt. is the optimum clay content. Finally, the results showed that thermal stability was significantly improved (20 °C) by the incorporation of these nano-clays, and similar improvements were observed for mechanical and rheological properties.

References

Abdellaoui H et al (2017) Laminated epoxy biocomposites based on clay and jute fibers. J Bionic Eng 14(2):379–389

Agag T, Koga T, Takeichi T (2001) Studies on thermal and mechanical properties of polyimide-clay nanocomposites. Polymer 42(8):3399–3408

Akin O, Tihminlioglu F (2018) Effect of organo-modified clay addition on properties of polyhydroxy butyrate homo and copolymers nanocomposite films for packaging applications. 26(3):1121–1132

Albano C, González J, Ichazo M, Kaiser D (1999) Thermal stability of blends of polyolefins and sisal fiber. Polym Degrad Stab 66(2):179–190

Amendola E et al (2012) Epoxy nanocomposites based on silylated montmorillonite: effect of the coupling agents structure on the mechanical properties. Macromolecules 6:33–36

Aowda SA, Jaffar Al-mulla EA, Baqir SJ (2011) Modification of montmorillonite, using different phosphonium salts, study their effect upon the structure. J Al-padisiyah Pure Sci 16:1–10

ASTM D 4092 – 01 (2013) Standard terminology for plastics: dynamic mechanical properties. ASTM Int 1–4

Bensalah H et al (2017) Mechanical, thermal, and rheological properties of polypropylene hybrid composites based clay and graphite. J Compos Mater 51(25):3563–3576

Bergaya F, Lagaly G (2013) General introduction: clays, clay minerals, and clay science. In: Handbook of clay science. Elsevier, Netherlands, pp 1–19

Bhat G, Hegde RR, Kamath MG, Deshpande B (2008) Nanoclay reinforced fibers and nonwovens. J Eng Fibers Fabr 3(3):22–34

Bhattacharya SS, Aadhar M (2014) Studies on preparation and analysis of organoclay nano particles. Res J Eng Sci 3(3):10–16

Bidsorkhi HC et al (2014) Mechanical, thermal and flammability properties of ethylene-vinyl acetate (EVA)/sepiolite nanocomposites. Polym Test 37:117–122

Boujmal R et al (2017) Alfa fibers/clay hybrid composites based on polypropylene. J Thermoplast Compos Mater 31(7):974–991

Carastan DJ et al (2013) Morphological evolution of oriented clay-containing block co-polymer nanocomposites under elongational flow. Eur Polym J 49(6):1391–1405

Carrado KA (2000) Synthetic organo- and polymer-clays: preparation, characterization, and materials applications. Appl Clay Sci 17(1–2):1–23

de Paiva LB, Morales AR, Díaz FRV (2008) Organoclays: properties, preparation and applications. Appl Clay Sci 42(1–2):8–24

Diagne M et al (2006) The effect of photo-oxidation on thermal and fire retardancy of polypropylene nanocomposites. J Mater Sci 41(21):7005–7010

Donescu D, Vuluga Z, Radovici C, Serban S (2008) Modification of organosilicate with silane coupling agents for polymer nanocomposites. Mater Plastice 45(4):305–309

Erden S, Ho K (2017) Composites science and engineering. Fiber technology for fiber-reinforced composites. Woodhead Publishing is an imprint of Elsevier

Essabir H et al (2016a) Structural, mechanical and thermal properties of bio-based hybrid composites from waste coir residues: fibers and shell particles. Mech Mater 93:134–144

Essabir H, Raji M, Bouh R (2016b) Nanoclay and natural fibers based hybrid composites: mechanical, morphological, thermal and rheological properties. In Nanoclay reinforced polymer composites, pp 29–49

Essabir H et al (2017) Morphological, thermal, mechanical, electrical and magnetic properties of ABS/PA6/SBR blends with Fe_3O_4 nano-particles. J Mater Sci Mater Electron 28(22):17120–17130

Fragiadakis D, Pissis P, Bokobza L (2005) Glass transition and molecular dynamics in poly (dimethylsiloxane)/silica nanocomposites. Polymer 46(16):6001–6008

Fujimori A, Kusaka J, Nomura R (2010) Formation and structure of organized molecular films for organo-modified montmorillonite and mixed monolayer behavior with poly(L-lactide). Polym Eng Sci 51(6):1–9

Gacitua EW, Aldo Ballerini A, Zhang J (2005) Polymer nanocomposites : synthetic and natural fillers. Maderas Ciencia y tecnología 7(3):159–178

Gao F (2004) Clay/polymer composites: the story. Mater Today 7(November):50–55

Gavrilko TA et al (2013) Molecular dynamics and phase transitions behavior of binary mixtures of fatty acids and cetyltrimethylammonium bromide as studied via davydov splitting of molecular vibrational modes. Ukrainian J Phys 58(7):636–645

González JA, Del M (2006) Bleaching of kaolins and clays by chlorination of iron and titanium. Appl Clay Sci 33:219–229

Guggenheim S et al (2006) Summary of recommendations of nomenclature committees relevant to clay mineralogy: report of Association Internationale Pour l'Etude Des Argiles (AIPEA) Nomenclature Committee for 2006. Clays Clay Miner 54:761–772

Hakeem KR, Jawaid M, Rashid U (2014) Fuel and energy abstracts. Biomass and bioenergy processing and properties. Springer, Berlin

He A et al (2010) Structural design of imidazolium and its application in PP/montmorillonite nanocomposites. Polym Degrad Stab 95(4):651–655. https://doi.org/10.1016/j.polymdegradstab.2009.12.003

Hoidy WH, Al-mulla EAJ (2013) Study of preparation for co-polymer nanocomposites using PLA/LDPE/CTAB modified clay. Iraqi Nat J Chem 49:61–72

Jeong E, Lim JW, Seo KW, Lee YS (2011) Effects of physicochemical treatments of illite on the thermo-mechanical properties and thermal stability of illite/epoxy composites. J Ind Eng Chem 17(1):77–82

Kokal I, Somer M, Notten PHL, Hintzen HT (2011) Sol–gel synthesis and lithium ion conductivity of $Li_7La_3Zr_2O_{12}$ with garnet-related type structure. Solid State Ionics 185(1):42–46

Kumar R, Yakabu MK, Anandjiwala RD (2010) Effect of montmorillonite clay on flax fabric reinforced poly lactic acid composites with amphiphilic additives. Compos A Appl Sci Manuf 41(11):1620–1627

Laaziz SA et al (2017) Bio-composites based on polylactic acid and argan nut shell: production and properties. Int J Biol Macromol 104:30–42

Laoutid F, Persenaire O, Bonnaud L, Dubois P (2013) Flame retardant polypropylene through the joint action of sepiolite and polyamide 6. Polym Degrad Stab 98(10):1972–1980

Leszczy A, Njuguna J, Pielichowski K, Banerjee JR (2007) Polymer/montmorillonite nanocomposites with improved thermal part II : thermal stability of montmorillonite nanocomposites based on different polymeric matrixes. Thermochim Acta 454(1):1–22

Li Y, Shimizu H (2005) Co-continuous polyamide 6 (PA6)/Acrylonitrile-Butadiene-Styrene (ABS) nanocomposites. Macromol Rapid Commun 26(9):710–715

Majeed K et al (2013) Potential materials for food packaging from nanoclay/natural fibres filled hybrid composites. Mater Des 46:391–410

Mansoori Y, Roojaei K, Zamanloo MR, Imanzadeh G (2012) Polymer-clay nanocomposites via chemical grafting of polyacrylonitrile onto cloisite 20A. Bull Mater Sci 35(7):1063–1070

Mejía A, García N, Guzmán J, Tiemblo P (2014) Surface modification of sepiolite nanofibers with PEG based compounds to prepare polymer electrolytes. Appl Clay Sci 95:265–274

Navrátilová Z, Wojtowicz P, Vaculíková L, Šugárková V (2007) Sorption of alkylammonium cations on montmorillonite. Acta Geodyn Geomater 4(3):59–65

Nazir MS et al (2016) Characteristic properties of nanoclays and characterization of nanoparticulates and nanocomposites. In Nanoclay reinforced polymer composites, pp 29–49. http://link.springer.com/10.1007/978-981-10-0950-1

Nekhlaoui S et al (2014) Fracture study of the composite using essential work of fracture method: PP–SEBS–g–MA/E1 clay. Mater Des 53:741–748

Nuzzo A et al (2014) Nanoparticle-induced co-continuity in immiscible polymer blends—a comparative study on bio-based PLA-PA11 blends filled with organoclay, sepiolite, and carbon nanotubes. Polymer 55(19):4908–4919

Oliveira M, Machado AV (2013) Preparation of polymer-based nanocomposites by different routes. In: Nanocomposites: synthesis, characterization and applications. NOVA Publishers, New York, pp 1–22
Pavlidou S, Papaspyrides CD (2008) A review on polymer–layered silicate nanocomposites. Prog Polym Sci 33:1119–1198
Pretschuh C, Schwarzinger C, Abdala AA, Vukusic S (2014) Characterization of conductive nanographite melamine composites. Open J Compos Mater 4:61–71
Raji M, Essabir H et al (2016a) Morphological, thermal, mechanical, and rheological properties of high density polyethylene reinforced with illite clay. Polym Polym Compos 16(2):101–113
Raji M, Mekhzoum MEM et al (2016b) Nanoclay modification and functionalization for nanocomposites development: effect on the structural, morphological, mechanical and rheological properties. In: Nanoclay reinforced polymer composites, pp 1–34
Raji M, Essabir H, Rodrigue D et al (2017a) Influence of graphene oxide and graphene nanosheet on the properties of polyvinylidene fluoride nanocomposites. https://doi.org/10.1002/pc.24292
Raji M, Essabir H, Bouhfid R, el kacem Qaiss A (2017b) Impact of chemical treatment and the manufacturing process on mechanical, thermal, and rheological properties of natural fibers-based composites. In: Handbook of composites from renewable materials. Wiley, Hoboken, pp 225–252
Santos KS et al (2013) The influence of screw configurations and feed mode on the dispersion of organoclay on PP. Polímymer 23(2):175–181
Singla P, Mehta R, Upadhyay SN (2012) Clay modification by the use of organic cations. Green Sustain Chem 2:21–25
Šupová M, Martynková GS, Barabaszová K (2011) Effect of nanofillers dispersion in polymer matrices: a review. Sci Adv Mater 3(1):1–25
Tamura K, Yokoyama S, Pascua CS, Yamada H (2008) New age of polymer nanocomposites containing dispersed high-aspect-ratio silicate nanolayers. Chem Mater 20(6):2242–2246
Tartaglione G, Tabuani D, Camino G, Moisio M (2008) PP and PBT composites filled with sepiolite: morphology and thermal behaviour. Compos Sci Technol 68(2):451–460
Tian H, Tagaya H (2007) Preparation, characterization and mechanical properties of the polylactide/perlite and the polylactide/montmorillonite composites. J Mater Sci 42(9): 3244–3250
Tjong SC (2006) Structural and mechanical properties of polymer nanocomposites. Mater Sci Eng R Rep 53(3–4):73–197
Usuki A (2002) Preparation and properties of EPDM—clay hybrids. Polymer 43(8):2185–2189
Vuluga Z et al (2014) The effect of polystyrene blocks content and of type of elastomer blocks on the properties of block copolymer/layered silicate nanocomposites. J Alloy Compd 616:569–576
Wang K et al (2013) Effect of talc content on the degradation of re-extruded polypropylene/talc composites. Polym Degrad Stab 98(7):1275–1286
Wu SH, Chen DH (2004) Synthesis of high-concentration Cu nanoparticles in aqueous CTAB solutions. J Colloid Interface Sci 273:165–169
Xie A et al (2011) Microstructure and antibacterial activity of phosphonium montmorillonites. Bull Korean Chem Soc 32(6):1936–1938
Xue W, He H, Zhu J, Yuan P (2007) FTIR investigation of CTAB-Al-Montmorillonite complexes. Spectrochim Acta Part A Mol Biomol Spectrosc 67(3–4):1030–1036
Yan W et al (2012) Morphology and mechanical properties of Acrylonitrile-Butadiene-Styrene (ABS)/polyamide 6 (PA6) nanocomposites prepared via melt mixing. J Macromol Sci Part B 51(1):70–82
Yürüdü C et al (2005) Synthesis and characterization of HDA/NaMMT organoclay. Bull Mater Sci 28(6):623–628
Zari N, Raji M, El Mghari H, Bouhfid R (2018) Nanoclay and polymer-based nanocomposites: materials for energy efficiency. In: Polymer-based nanocomposites for energy and environmental applications. Woodhead, UK, pp 75–103
Zeng QH, Yu AB, Lu GQ, Paul DR (2005) Clay-based polymer nanocomposites: research and commercial development. J Nanosci Nanotechnol 5:1574–1592

Zhang Z, Zhang J, Liao L, Xia Z (2013) Synergistic effect of cationic and anionic surfactants for the modification of Ca-montmorillonite. Mater Res Bull 48(5):1811–1816

Zhao Y, Abdullayev E, Vasiliev Ae, Lvov Y (2013) Halloysite nanotubule clay for efficient water purification. J Colloid Interface Sci 406(June):121–129

Zotti A et al (2014) Effect of sepiolite filler on mechanical behaviour of a bisphenol A-based epoxy system. Compos B Eng 67:400–409

Zýková J, Kalendová A, Kovářová L, Maláč J (2009) Influence of intercalation agents on the thermal stability of Pvc/clay. Nanocon 20(10):1–4